Commun Nonlinear Sci Numer Simulat 19 (2014) 164–172

Contents lists available at SciVerse ScienceDirect

Commun Nonlinear Sci Numer Simulat

journal homepage: www.elsevier.com/locate/cnsns

Dynamic range in a neuron network with electrical and chemical synapses

R.L. Viana [a,*], F.S. Borges [b], K.C. Iarosz [b], A.M. Batista [c], S.R. Lopes [a], I.L. Caldas [d]

[a] Departamento de Física, Universidade Federal do Paraná, 81531-990 Curitiba, PR, Brazil
[b] Pós-Graduação em Ciências, Universidade Estadual de Ponta Grossa, 84030-900 Ponta Grossa, PR, Brazil
[c] Departamento de Matemática e Estatística, Universidade Estadual de Ponta Grossa, 84030-900 Ponta Grossa, PR, Brazil
[d] Instituto de Física, Universidade de São Paulo, Caixa Postal 66316, 05315-970 São Paulo, SP, Brazil

ARTICLE INFO

Article history:
Received 8 November 2012
Received in revised form 14 March 2013
Accepted 4 June 2013
Available online 17 June 2013

Keywords:
Dynamic range
Cellular automata
Neural network

ABSTRACT

The dynamic range is the logarithmic difference between maximum and minimum levels of sensation produced by known stimuli. In the human sensory systems the dynamic ranges are typically larger than for single neurons, this amplification being essentially a collective effect of the neural network. We investigated the dynamic range exhibited by a cellular automaton network with electrical and chemical synapses, when the stimuli are modelled by a Poisson process of suprathreshold events of stereotyped unit amplitude and the neuron response is its average firing rate.

© 2013 Elsevier B.V. All rights reserved.

1. Introduction

The quantitative characterization of the sensation we assign to a given stimulus was one of the key problems in Psychophysics [1]. Weber and Fechner proposed, in the 19th century, that the relationship between stimuli and response was logarithmic, rather than linear: the magnitude P of the sensation related to a given stimulus depends on the magnitude I of the stimulus itself by $P \sim \ln I$ [2].

In the mid-1950s, Stevens has proposed a more general stimulus–response theory based on a power-law $P \sim I^m$. This is an empirical mathematical statement obtained by electrophysiological experiments [3]. The exponent m has been found to be 0.67 for loudness, 0.33 to 1.0 for brighness, 0.8 to 1.4 for taste, and 0.7 to 1.6 for warmth, just to give some examples [1].

Due to anatomical and physiological limitations of our senses, any quantitative relationship between stimulus and sensation must have upper and lower bounds corresponding, respectively, to the largest and the smallest values of the response, measured by some changeable quantity. The dynamic range is the logarithm of the difference between the largest and the smallest value of this quantity, and is usually expressed in decibels (dB). For example, the human senses of sight and hearing have relatively large values of the dynamic range, of 90 dB and 100 dB, respectively [4]. In terms of a general stimulus–response relation the dynamic range is the interval over which a power-law (Stevens law) can be fitted.

Experimental evidence points out that the dynamic range of a single neuron is substantially less than the dynamic range observed at the macroscopic level [5]. As an example, in the case of mouse olfactory system, isolated receptor neurons exposed to odorant chemicals have a dynamic range of the order of 10 dB [6,7]. On the other hand, the corresponding

* Corresponding author.
E-mail address: viana@fisica.ufpr.br (R.L. Viana).

1007-5704/$ - see front matter © 2013 Elsevier B.V. All rights reserved.
http://dx.doi.org/10.1016/j.cnsns.2013.06.003

dendro-dendritic neural network in the glomeruli exhibits a dynamic range of about 30 dB [8,9]. Therefore the enhanced dynamic range at the macroscopic level is a collective effect caused by the network structure.

In terms of mathematical descriptions of both neuronal activity and neuron connective architecture, it is interesting to verify how the dynamic range of a given neuronal network depend on its characteristic parameters. From the neuronal point of view the response of a neuron to a given stimulus can be represented by its firing rate, or the number of spikes it generates per unit time. Those spikes are produced after injection of stimuli represented by an injected current. The external stimuli on an individual neuron can be thought as a random sequence of injected signals with a given average input rate. Hence, from the microscopic point of view, the stimulus–response curve of a neuron would be its input rate-firing rate relationship. The dynamic range can be obtained from this relationship by considering the amplitude for which a power-law scaling holds.

The mechanism underlying the enhancement of the dynamic range in a neuronal network has been described by Copelli and coworkers as collective nonlinear wave properties of arrays made of coupled excitable elements [10]. Such media support the formation and annihilation of nonlinear waves that not only enhance the dynamic range but also the sensitivity. These facts were observed using cellular automata, which are simple spatially extended discrete models which allow for essential features necessary to describe active media, like excitability and refractoriness (their results were also confirmed by networks of realistic neurons described by Hodgkin–Huxley equations). The dynamical range in this model was shown to be maximal at the critical point of a non-equilibrium phase transition [5].

In the cellular automaton model used by Copelli et al. each element represents a neuron which can be in two states: a resting and a spiking one, following deterministic rules for its time evolution. The external input signal is modeled by a Poisson process of suprathreshold events with a given average time rate. The coupling between neurons in this model considers the effect of nearest neighbors, hence it mimics electrical (gap junction) synapses. Such gap junction coupling type is consistent with experimental findings that projection cells in sensory systems are coupled via dendro-dendritic electrical synapses, as α-ganglionar cells in the retina and mitral cells in the olfactory bulb [11–13].

However, in neuronal networks there are also chemical synapses, by which one neuron releases neurotransmitter molecules into a small cleft that is adjacent to another neuron. These molecules then bind to the neuroreceptors on the receiving cell's side of the synaptic cleft. Hence we can model chemical synapses in an artificial network by considering non-local connections among randomly selected neurons with a given probability, i.e. neurons which are not nearest neighbors. In a recent work we have modified the model of Copelli et al. by introducing nonlocal connections in this way [14].

This procedure of randomly adding non-local connections in order to model chemical synapses generates networks possessing the so-called small-world property. A small-world network has typically an average distance between sites comparable to the value it would take on a random network, while retaining an appreciable degree of clustering, as in regular networks [15]. There are many examples of neuronal networks exhibiting the small-world property, the more famous being the worm *Caenorhabditis elegans*, which has 282 neurons with *ca.* 6000 synapses [16]. Functional networks for the human brain using magnetoencephalographic data have been also found to have the small-world property [17].

Watts and Strogatz obtained small-world networks from an otherwise regular lattice with local connections, to which nonlocal connections were added by randomly rewiring a small fraction of the local connections [15]. An alternative procedure was proposed by Newman and Watts, who inserted randomly chosen shortcuts in a regular lattice, instead of re-wiring local interactions into non-local ones [18]. For small values of the probability the networks obtained according the Watts–Strogatz and Newman–Watts procedures have similar statistical properties.

The properties of networks in the strong dilution limit, i.e. with nonlocal shortcuts randomly chosen with a very small probability, have been studied recently. In such sparse networks it is possible to observe nontrivial collective dynamics (even in the thermodynamical limit) for finite connectivity, by considering a number of different models, as leaky integrate-and-fire neurons and phase oscillators of the Stuart-Landau type [19,20]. The nontrivial collective dynamics observed in these works refers to a transition from an asynchronous behavior to a partially synchronized one characterized by coherent periodic activity. Small-world networks of slightly different bursting neurons described by discrete-time maps can present synchronized bursting if the coupling strength is large enough, presenting features of a Kuramoto-like transition between a non-synchronized and a synchronized bursting regime [21]. It is possible to observe such a synchronization transition even if the phase oscillators are noisy, exhibiting stochastic behavior, in this case the small-world network being dense, with a relatively large probability of nonlinear shortcuts [22]. Finally, cellular automata with local connections are able to exhibit a kind of synchronization phenomenon if suitable measures are introduced for distinguishing different patterns, as the Boolean distance [23] and the Hamming distance [24].

In this paper we analyze the dynamic range of the cellular automaton model of Copelli et al. with both electrical and chemical synapses, the latter being modelled as nonlocal connections randomly chosen according to a given probability, in accordance with the Newman–Watts procedure for generating small-world networks. In particular, we investigate how the dynamic range of the network varies with the parameters of the cellular automaton. We observed that the presence of chemical synapses, as long as the probability of nonlocal shortcuts is small enough, maintains the power-law stimulus–response relationship. We found that the addition of chemical synapses increases the dynamical range, thus enhancing the effect already shown by networks with electric (gap-junction) synapses only [10].

The rest of the paper is organized as follows: in the second section we describe a theoretical model for the neuronal network with electrical and chemical synapses. Section 3 brings the studies about the dynamic range obtained from numerical simulations. Section 4 contains our conclusions.

2. Cellular automaton model of spiking neurons

Usual models of neuronal networks (like the Hodgkin–Huxley model) employ a set of ordinary differential equations describing the excitable dynamics of a neuron under the influence of an injected current which can be both an external stimulus or the result of synaptic coupling with other neurons in the assembly. Further simplification results from discretizing the time variable, like the Rulkov map, what yields a coupled map lattice. If, moreover, we discretize also the state variable describing the neuron state, there results a cellular automaton. In spite of its structural simplicity, it can generate complex dynamics, still retaining some essential features of the neuronal assembly being modeled.

The neural network model proposed by Copelli et al. consists of a μ-state cellular automaton with excitable elements described by the variables x_i, $i = 1, 2, \ldots, N$, representing neuronal activity [10]. The latter consists of spikes which last the order of 1 ms, what provides a characteristic time scale of 1 ms per time step, used to discretize the variable t.

The variable x represents the membrane potential of the neuron. The resting state, in which the neuron is quiescent, is characterized by $x_i = 0$, corresponding to a resting potential of about -70 mV [25]. A spiking neuron has $x_i = 1$, hence x represents the membrane potential of the neuron (during a spike the membrane potential reaches a peak value of +30 mV). After the spike the membrane potential is reset and the neuron enters into a refractory period, during which it does not spike. We model this situation by assuming that the spiking neuron x_i may present the following values: $\{1, 2, \ldots, \mu - 1\}$. If a stimulus arrives while the neuron is in a resting state ($x_i = 0$) it spikes ($x_i = 1$), remaining insensitive during $\mu - 2$ time steps. Hence $\mu - 2$ stands for the refractory period during which the neuron cannot spike even if it receives an external input.

Once it is in its resting state, a neuron can spike when it receives stimulus as a result of an external input signal or through its synapses. Let $h_i \in \{0, 1\}$ denote the external stimulus. Then the rules for time evolution of the cellular automaton are [10]:

- For $x_i(t) = 0$, then $x_i(t + 1) = h_i(t)$, hence a neuron spikes only if stimulated in its resting state.
- For $x_i \neq 0$, then $x_i(t + 1) = [x_i(t) + 1] \pmod{\mu}$. This means that, once it has spiked, the neuron becomes refractory during $\mu - 2$ time steps.

The external input signal acting on the ith neuron is modelled by a Poisson process of suprathreshold events of stereotyped unit amplitude

$$\Im_i(t) = \sum_n \delta(t, t_n^{(i)}), \tag{1}$$

where $\delta(a, b)$ is the Kronecker delta, meaning that the external inputs are applied at well-defined times $t_n^{(i)}$, with $n = 1, 2, \ldots$. The time intervals between two consecutive inputs, namely $\Delta t = t_{n+1}^{(i)} - t_n^{(i)}$, are distributed according to an Poisson distribution with average input rate r. This means that the inputs are distributed with a probability per time step equal to [5]

$$\lambda(r) = 1 - e^{-r\Delta t}. \tag{2}$$

Without stimuli the neurons eventually go to their resting state $x_i = 0$. When the neurons are uncoupled the stimulus is given by

$$h_i(t) = \delta(\Im_i(t), 1). \tag{3}$$

A cellular automaton network with N neurons is formed by coupling both adjacent (nearest neighbor) and distant neurons to the ith neuron. These contributions are integrated into the external stimulus $h_i(t)$ that includes both the synaptic currents from the coupling and the external inputs. Hence $h_i(t)$ will be nonzero if any of the neighbor neurons are spiking and/or there is an external input at the time t.

We can model such a complex stimulus (external input plus the synaptic connections) by the following expression

$$h_i(t) = 1 - [1 - \delta(\Im_i(t), 1)] \prod_{j=\pm 1} [1 - \delta(x_{i+j}(t), 1)] \times [1 - \delta(x_{i-1}(t), 1)][1 - \delta(x_{i+1}(t), 1)] \prod_{j \in I} [1 - a_{ij}\delta(x_j(t - \tau), 1)]. \tag{4}$$

The expression (4) contains two coupling terms: the first represents the electrical synapses connecting the nearest neighbor cells in the network. This term is nonzero whenever the nearest neighbors are spiking and/or the external input is nonzero. The second term in Eq. (4) correspond to chemical synapses involving the releasing of neurotransmitters which diffuse through the synaptic cleft and bind to neuroreceptors of the receiving neuron. Such couplings can thus extend to non-nearest neighbors of a given cell and we model them as non-local shortcuts in the network, randomly chosen with a probability p from a uniform distribution [26].

This procedure is similar to that used by Newman and Watts to generate small-world networks out of regular coupled lattices [18]. We have chosen this probability to be given by $p = M/(N^2 - 3N + 2)$, where M be the number of non-local shortcuts inserted in a regular lattice of N sites. In Eq. (4), the symbol I denote the set comprising those randomly chosen neurons. The connectivity among these neurons can be described by an adjacency matrix a_{ij} whose entries are 0 (1) if the ith and jth neurons are not (are) connected by chemical synapses.

The network has local connections associated with electrical synapses which are fast and bidirectional, and non-local connections representing chemical synapses which are unidirectional and slower than electrical synapses. In order to cope with this difference we have introduced a time delay τ in the chemical synapses coupling term. Fig. 1(a) shows a schematic

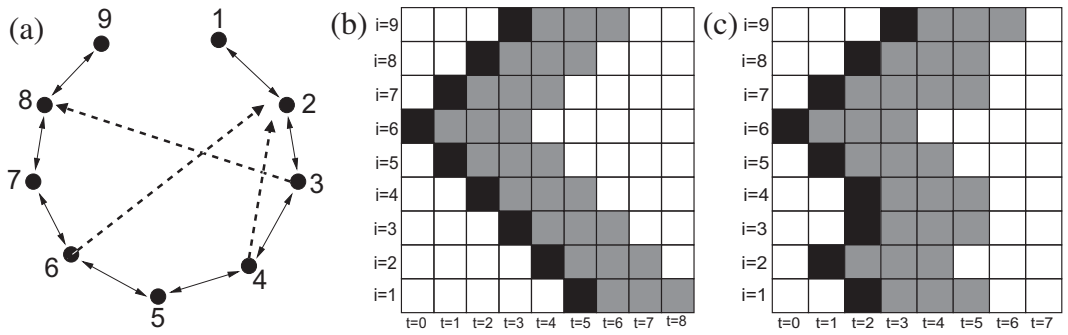

Fig. 1. (a) Schematic representation of the neural network with electrical and chemical synapses; (b) space–time evolution of the system with no chemical synapses and refractory period $\mu = 5$. Resting, spiking and refractory neurons are depicted in white, black, and grey, respectively. (c) The same as in (b), but with chemical synapses randomly chosen with probability $p = 0.053$ and time delay $\tau = 0$.

representation of a CA neural network with $N = 9$ neurons, each of them with $\mu = 5$ refractory states, and free boundary conditions. The electrical synapses are supposed to be bidirectional (solid arrows), whereas the chemical synapses are unidirectional (dashed arrows). The corresponding connectivity matrix is such that the electrical synapses are responsible for the two secondary diagonals straddling the main diagonal of zeroes (since we exclude self-interactions), and the chemical synapses are nonzero elements sparsely distributed along the matrix.

The case with electrical couplings only (and thus no time delay whatsoever) is illustrated by Fig. 1(b), where we depict the space–time evolution of the cellular automaton with the following initial condition: $x_6(0) = 1$ and $x_i(0) = 0$ for $i \neq 6$. We denote resting neurons ($x_i = 0$) by blank squares, spiking neurons ($x_i = 1$) by black squares, and refractory neurons ($x_i = 2, \ldots 5$) by grey. According to the cellular automaton rules a single spiking neuron generates a spiking "wave" along the lattice which dies out. The chemical synapses are included as $M = 3$ randomly chosen shortcuts with a probability $p = 0.053$ and no time delay. As shown by Fig. 1(c), one effect of including chemical synapses is to create a more complex firing wave pattern.

The injected signals on the coupled neurons are randomly chosen according to a Poisson distribution with average input rate r. The neuron response to this stereotyped stimuli can be obtained through the density of spiking neurons

$$\rho(t) = \frac{1}{N}\sum_{i=1}^{N}\delta(x_i(t), 1), \tag{5}$$

so that we compute the time averaged density of firing neurons, or the average firing rate

$$F = \overline{\rho(t)} = \frac{1}{T}\sum_{t=1}^{T}\rho(t), \tag{6}$$

where T is the time window chosen for the average.

If there is injected signal ($r = 100$) and small time delay ($\tau = 10$), the time evolution of the spiking neuron density of a network with $N = 10^4$ neurons and electrical and chemical synapses may be a complex periodic pattern (Fig. 2(a)). As revealed by the corresponding power spectrum, this periodic behavior exhibits a fundamental frequency equal to 0.2 and one harmonic at 0.4 (Fig. 2(b)). This periodic behavior is corrupted by increasing the time delay to $\tau = 500$ (Fig. 2(c)). The result is a rather irregular behavior, with the main frequencies embedded in a broadband noise background (Fig. 2(d)). In both cases, we computed a time-averaged firing rate, yielding $F = 0.2$ and 0.192 for the cases depicted in Fig. 2(a) and (c), respectively.

The effect of increasing the probability of nonlocal shortcuts, i.e. the fraction of chemical synapses in the model, can be illustrated in Fig. 3, where we have considered the time evolution of the density ρ of firing neurons for three different values of p. Fig. 3(a), obtained with $p = 0$ (no nonlocal shortcuts, or electrical synapses only) shows a few firing waves which disappear after some lifetime due to collisions and the damping effect of the refractory period of each neuron. Accordingly the density of the firing neurons remains small (less than 4% in average for the time period considered) (Fig. 3(b)). If chemical synapses are included with a small probability (Fig. 3(c)) the firing waves become occur much more frequently leading to an enhanced density of firing neurons (with peak values of almost 20%) (Fig. 3(d)). Finally, for large p, what brings us to a globally coupled lattice where all neurons connect with other ones, there are no longer firing waves but rather a nearly synchronized firing (Fig. 3(e)), which makes the density of firing neurons to undergo regular oscillations and with maxima larger than 30% (Fig. 3(f)). The conclusion we reach is that the increase of p makes the firing more synchronous and the density of firing neurons has large-amplitude oscillations.

In order to investigate the role of electrical and chemical synapses on the firing properties of the system we have considered in Fig. 4 a cellular automaton without local coupling (electric or gap-junction synapses) and the time evolution of the density ρ of firing neurons for different values of p. In Fig. 4(a), obtained with $p = 0$ (no local or nonlocal connections do

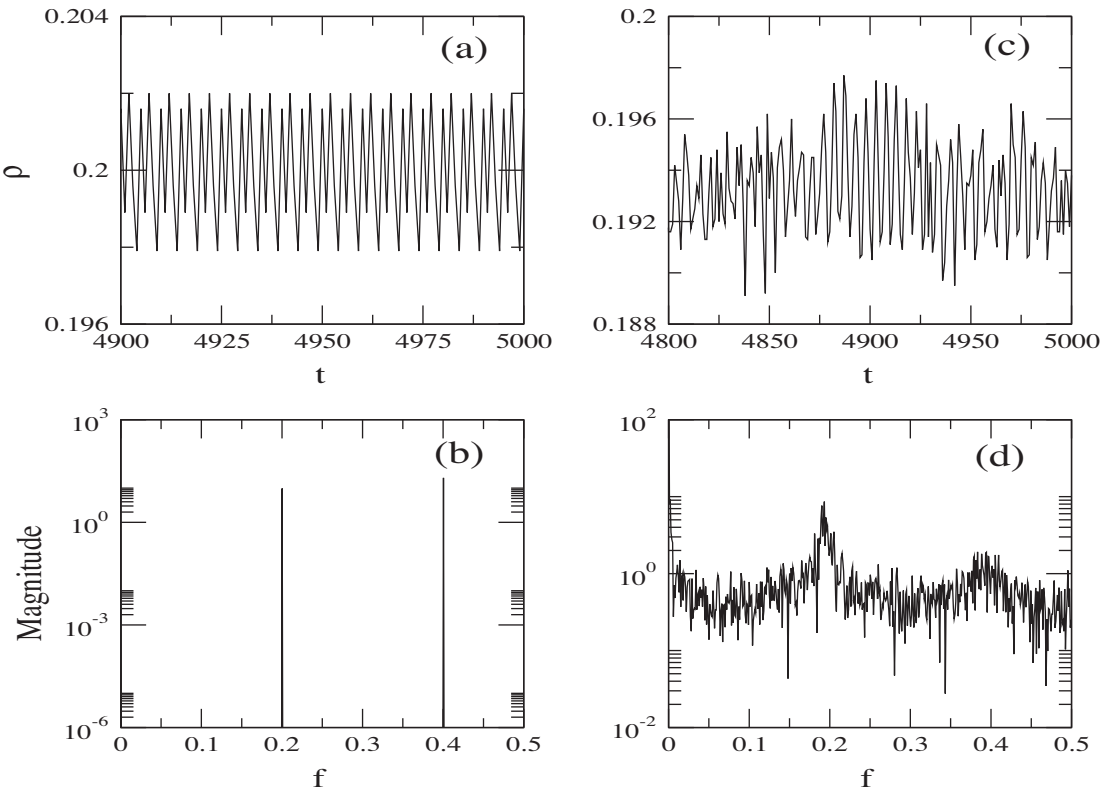

Fig. 2. Time evolution of the density of spiking neurons for a neural network with $N = 10^4$ neurons, with electrical and chemical synapses randomly chosen with probability $p = 10^{-5}$ and external stimuli with rate $r = 100$. We consider the time delay equal to (a) $\tau = 10$ and (c) $\tau = 500$. (b) and (d) are the power spectra related to (a) and (c), respectively.

exist), the uncoupled neurons only fire due to the external stimuli, if any. Hence only a handful of neurons are actually firing. The density is small and highly fluctuating (Fig. 4(b)). When chemical synapses are included with a small probability (Fig. 4(c)) there is partial synchronization of firing, but no firing waves, which is probably due to the absence of local connections. Even so, this results in a much higher density of firing neurons, presenting both small and large fluctuations (Fig. 4(d)). In the case $p = 1$, equivalent to a globally coupled network, we have again synchronized firing (Fig. 4(e)), and the density of firing neurons displays an alternacy between large peaks and no activity at all, a characteristic feature of a global synchronized behavior (Fig. 4(f)). Hence the absence of electrical synapses makes the firing behavior more prone to synchronization, with absence of firing waves. This makes the density of firing neurons to evolve in a spike-like fashion, instead of a broadband fluctuation like in the case where there are both electrical and chemical synapses.

3. Dynamic range

We can study the stimulus–response relationship of the network by plotting its average firing rate F versus the average input rate r. For a network with electrical synapses only ($p = 0$) this relation is well-fitted by a power-law, as in Stevens' law, $F \sim r^m$, with exponent $m = 0.5$. If we include chemical synapses with a given probability p and time delay τ, the same scaling is observed, but with different value of the exponent. Fixing τ and varying the probability we can see in Fig. 5 a saturation value of the average firing rate when p increases, where this saturation occurs for small average input rate. As a matter of fact, considering $\tau = 500$ and $p = 10^{-8}$ (circles) we obtain a slope of 0.53 while for $p = 10^{-6}$ (squares) a slope of 1.27.

The origin of this saturation behavior lies in the refractory period experienced by each neuron in the cellular automaton model. During this refractory period the neuron does not fire even when the rules for updating the lattice would permit so. Hence if the input rate is too high, the input pulses will most likely perturb neuron during its refractory phase and thus the neuron will not respond to these inputs, characterizing saturating behavior. Since the refractory period is equal to μ time units, the maximum firing rate can be estimated as $F_{max} \sim 1/\mu$, which is equal to 0.2 for $\mu = 5$. This value agrees with the large r limit in Fig. 5, the lower curve describes a more gently rise, and the saturation occurs for larger input rates, although with the same maximum firing rate. This observation is also confirmed by the forthcoming results.

Fig. 6 displays the behavior of the average firing rate (values are indicated by a color-scale) for the parameter ranges investigated in this work. In Fig. 6(a), for small values of the time delay the average firing rate increases until 0.2 with

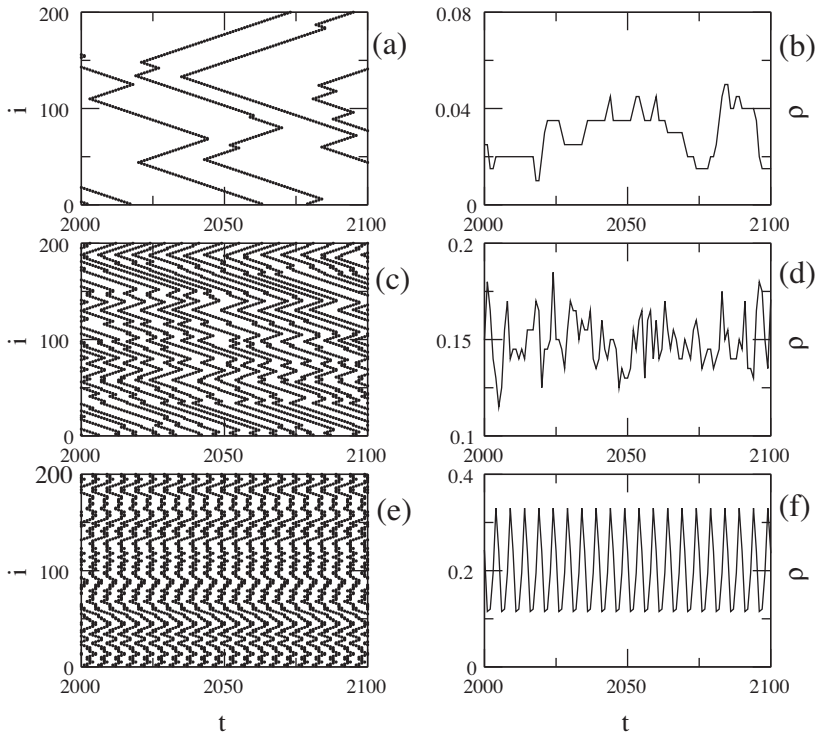

Fig. 3. Space–time evolution of the cellular automaton with $N = 200$ neurons, input rate $r = 1$, time delay $\tau = 500$ and probability of nonlinear connections $p = 0$ (a), 0.001 (b) and 0.25 (c). (b), (d) and (f) show the time evolution of the firing neuron density for (a), (b) and (c), respectively.

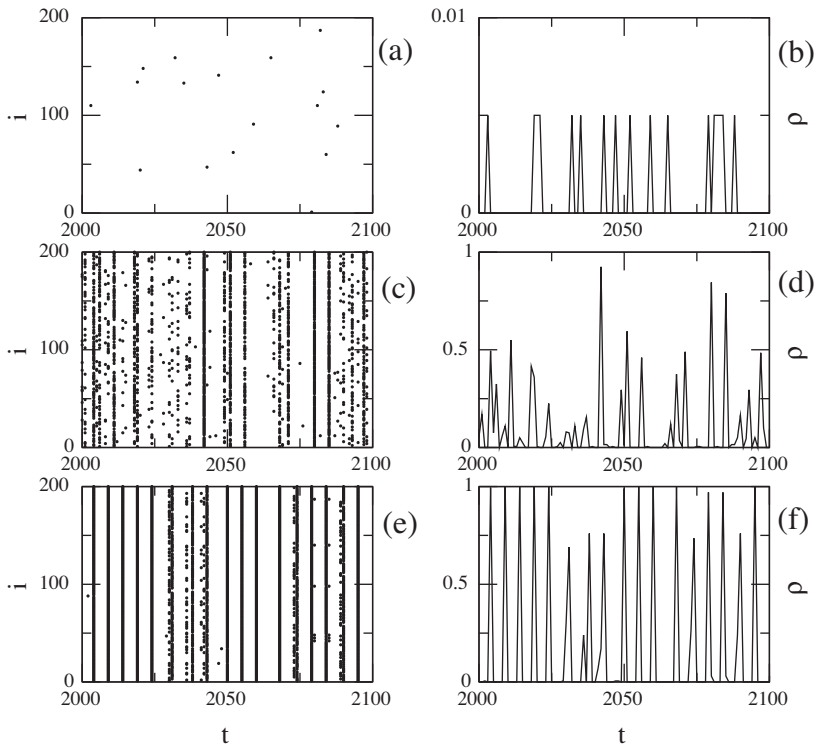

Fig. 4. Space–time evolution of the cellular automaton with $N = 200$ neurons, input rate $r = 1$, time delay $\tau = 500$ and probability of nonlinear connections $p = 0$ (a), 0.02 (b) and 0.25 (c). (b), (d) and (f) show the time evolution of the firing neuron density for (a), (b) and (c), respectively.

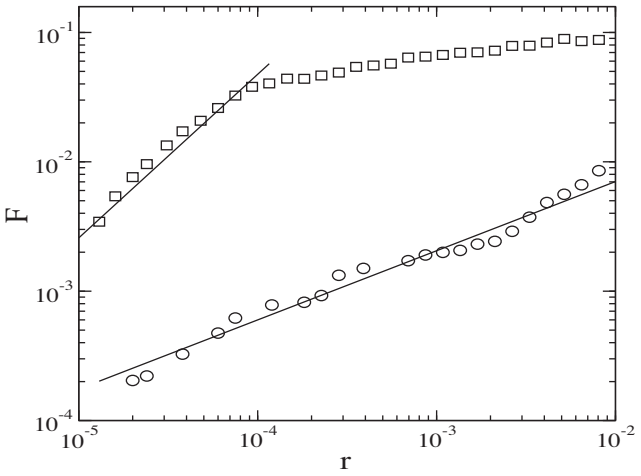

Fig. 5. Average firing rate as a function of the average input rate for a neural network with $N = 10^4$ neurons. We consider $\tau = 500$ and different chemical synapses randomly chosen with probability: $p = 10^{-8}$ (circles) and $p = 10^{-6}$ (squares). The solid lines have slope 0.53 and 1.27, respectively.

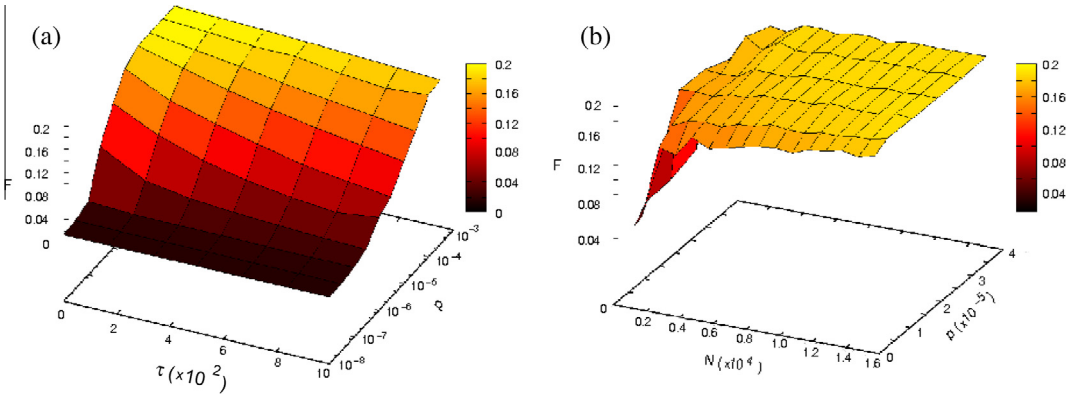

Fig. 6. (a) Average firing rate as a function of the time delay (τ) and of the probability (p), considering $N = 10^4$ and $r = 10^{-1}$. (b) $\tau = 500$ and $r = 10^{-1}$.

the probability p. For a large τ F also grows monotonically with increasing p, but the growth rate is smaller. Concerning the Fig. 6(b) F rises sharply with the network size. For network sizes greater than $N \sim 2000$, $\tau = 500$ and $r = 10^{-1}$ we observe that the values of the average firing rate remain constant. In both cases the maximum firing rate agrees with the theoretical value $1/\mu$.

The general relationship between F and r is a sigmoid-shaped function, due to saturation effects: for large r the neurons are not responsive because of their refractory periods, and for small r the external inputs are so rare that the system loses any memory of the previous stimuli and responds in very much the same way. We now consider this relationship for a network with relatively few nonlocal shortcuts and a nonzero time delay. A network with τ fixed and increasing p exhibits a power-law dependence of F on r with an exponent that increases with p. For $\tau = 500$ and $p = 10^{-8}$ the exponent is 0.53 (circles), whereas if $p = 10^{-6}$ (squares) the exponent increases to 1.27 (Fig. 5). Therefore, due to chemical synapses it is possible to obtain different values for the scaling exponent.

We can obtain the dynamic range by choosing the interval for which a power-law fit holds, or

$$\Delta = 10\log_{10}\left(\frac{r_H}{r_L}\right), \tag{7}$$

in which r_L and r_H are the average input rates obtained for 10% and 90% of the maximum average firing rate F_{max}, respectively, without loss of generality. Fig. 7 shows the variation of the average firing rate with the average input rate over six orders of magnitude for a network of $N = 10^4$ neurons, with electrical synapses only (Fig. 7(a)) and electrical and chemical synapses randomly chosen with probability $p = 10^{-7}$ and time delay $\tau = 500$ (Fig. 7(b)). In both cases the maximum average firing rate was kept $F_{max} = 0.2$, such that the dynamic ranges are the intervals for which F is between 0.1 and 0.9 of this maximum response.

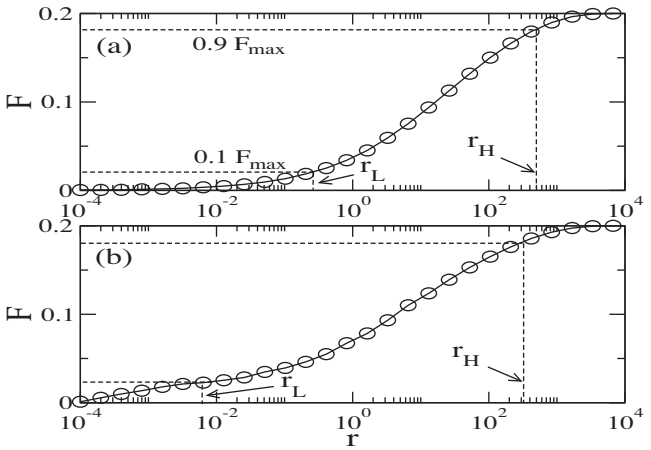

Fig. 7. Average firing rate as a function of the average input rate in a neural network with $N = 10^4$ neurons and (a) electrical synapses only ($p = 0$); (b) chemical synapses randomly chosen with probability $p = 10^{-7}$ and time delay $\tau = 500$.

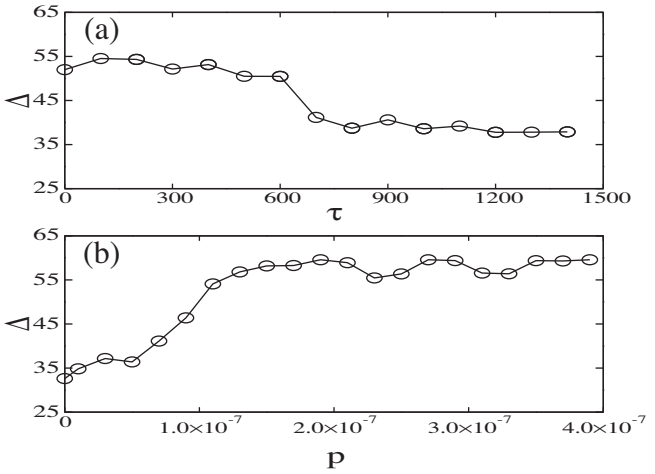

Fig. 8. Dynamic range in a neural network with $N = 10^4$ neurons and electrical and chemical synapses as a function of (a) time delay, for $p = 10^{-7}$; (b) probability of nonlocal shortcuts with $\tau = 500$.

When defining the dynamic range we have, rather arbitrarily, chosen lower and upper bounds as 90% and 10%, respectively, of the maximum firing rate. As long as the scaling region continues to be well fit by a power law, though, these values can vary a little bit, like 85% and 15% for example. Such small changes are not likely to affect our results.

In the presence of only electrical synapses the values of r_H and r_L are given, respectively, by 510.98 and 0.28, yielding a dynamic range of $\Delta = 32.6$. As we include the chemical synapses with a given probability $p = 10^{-7}$ and time delay $\tau = 500$ the values of both r_H and r_L decrease to 278 and 0.0025, respectively. As a result, in this case the dynamic range is equal to 50.46.

Increasing τ the dynamic range was found to actually decrease from ~ 50 to 30, which is the value obtained for a lattice with electrical synapses only (Fig. 8(a)). This is hardly surprising, though, since we already found that a large time delay brings the network with chemical synapses closer to a critical network with electrical synapses only. We remark that the minimum value of the average firing rate was found to be larger than $0.1F_{max}$ when the number of chemical synapses (i.e., the value of p) increases. As a result, for larger p we have not observed a value for r_L, whereas r_H remains constant. However, since r_L decreases more than r_H, there follows that the dynamic range increases. In fact, keeping the time delay constant (in $\tau = 500$) and increasing the shortcut probability the dynamic range was found to double from ~ 30 to 60 (Fig. 8(b)).

4. Conclusions

There is experimental evidence that the amplified dynamic range observed in human sensory organs is a collective effect caused by the complexity inherent to the neural network spatio-temporal dynamics. In order to investigate this collective

phenomenon it is necessary to use computationally fast models, like cellular automata, which still retain important features of more complicated models like refractory periods and time delays.

Although most of the synapses of neurons involved in sensory organs are of electrical origin (gap junctions), the effect of chemical synapses is an important factor to take into account in more realistic models. Chemical synapses involve interactions among neurons more or less distant and thus can be modelled, in cellular automata, by including nonlocal shortcuts randomly chosen with a given probability.

We have found that the presence of chemical synapses does not alter qualitatively the stimulus–response curve of the network, which is, in the macroscopic level of human senses, described by Stevens' power-law scaling. The absence of chemical synapses leads to a power-law exponent of 0.5, which changes in the presence of chemical synapses. However, if we also include a time delay in the chemical synapses, for large enough values of it the power-law exponent asymptotes to 0.5. By varying both the probability and time delay it is possible, at least in principle, to tailor the neural network to exhibit a power-law dependence with a desired exponent.

Another conclusion from our work is that the dynamic range exhibited by the network actually increases with the number of chemical synapses, and may be doubled by adding a modest number of nonlocal shortcuts to an otherwise purely electrically coupled network. If this probability is fixed and the time delay is increased, however, the opposite occurs and the dynamic range decreases. Hence a network with chemical synapses and large dynamic range should contain a considerable number of nonlocal shortcuts, but with a time delay not too large.

We believe that the general trends observed in our simple model, related to the enhancement and adjustability of the dynamic range, could be also verified in more sophisticated models with coupled differential equations, like the Hodgkin–Huxley equations [27], in which the chemical synapses may be modelled by a rapidly diffusing neurotransmitter in the interneuron environment [28].

Acknowledgments

This work was made possible with the help of CNPq, CAPES, FAPESP, and Fundação Araucária (Brazilian Government Agencies).

References

[1] Stevens SS. Psychophysics: introduction to its perceptual neural and social prospects. New Jersey: Transaction Publisher; 2008.
[2] Chialvo DR. Psychophysics: are our senses critical? Nat Phys 2006;2:301–2.
[3] Hubbard TL. Memory psychophysics. Psych Res Psych Fors 1994;56:237–50.
[4] Siegel GM, Schork Jr EJ, Pick Jr HL, Garter SR. Parameters of auditory feedback. J Speech Hear Res 1982;25:473–5.
[5] Kinouchi O, Copelli M. Optimal dynamical range of excitable networks at criticality. Nat Phys 2006;2:348–51.
[6] Reisert J, Matthews HR. Response properties of isolated mouse olfactory receptor cells. J Physiol 2001;530:113–22.
[7] Tomaru A, Kurahashi T. Mechanisms determining the dynamic range of the bullfrog olfactory receptor cell. J Neurophysiol 2005;93:1880–8.
[8] Wachowiak M, Cohen LB. Representation of odorants by receptor neuron input to the mouse olfactory bulb. Neuron 2001;32:723–35.
[9] Fried HU, Fuss SH, Korsching SI. Selective imaging of presynaptic activity in the mouse olfactory bulb shows concentration and structure dependence of odor responses in identified glomeruli. Proc Natl Acad Sci USA 2002;99:3222–7.
[10] Copelli M, Roque AC, Oliveira RF, Kinouchi O. Physics of psychophysics: Stevens and Weber–Fechner laws are transfer functions of excitable media. Phys Rev E 2002;65:060901(R).
[11] Kosaka T, Deans MR, Paul DL, Kosaka K. Neuronal gap junctions in the mouse main olfactory bulb: morphological analyses on transgenic mice. Neuroscience 2005;134:757–69.
[12] Migliore M, Hines ML, Shepherd GM. The role of distal dendritic gap junctions in synchronization of mitral cell axonal output. J Comput Neurosci 2005;18:151–61.
[13] Christie JM, Bark C, Hormudzi SG, Helbig I, Monyer H, Westbrook GL. Connexin36-mediated spike synchrony in olfactory bulb glomeruli. Neuron 2005;46:761–72.
[14] Iarosz KC, Batista AM, Viana RL, Lopes SR, Caldas IL, Penna TJP. The influence of connectivity on the firing rate in a neuronal network with electrical and chemical synapses. Physica A 2012;391:819–27.
[15] Watts DJ, Strogatz SH. Collective dynamics of 'small-world' networks. Nature 1998;393:440–2.
[16] Varshney LR, Chen BL, Paniagua E, Hall DH, Chklkovskii DB. Structural properties of the *Caenorhabditis Elegans* Neuronal Network. PLOS Comput Biol 2011;7:e1001066.
[17] Scannell JW, Young MP. The connectional organization of neural systems in the cat cerebral cortex. Curr Biol 1993;3:191-00;
Scannell JW, Blakemore C, Young MP. Analysis of connectivity in the cat cerebral cortex. J Neurosci 1995;15:1463–83.
[18] Newman MEJ, Watts DJ. Renormalization group analysis of the small-world network model. Phys Lett A 1999;263:341–6.
[19] Luccioli S, Olmi S, Politi A, Torcini A. Collective dynamics in sparse networks. Phys Rev Lett 2012;109:138103.
[20] Tattini L, Olmi S, Torcini A. Coherent periodic activity in excitatory Erd–Reniy neural networks. Chaos 2012;22:023133.
[21] Batista CAS, Batista AM, Pontes JAC, Viana RL, Lopes SR. Chaotic phase synchronization in scale-free networks of bursting neurons. Phys Rev E 2007;76:016218.
[22] Sonnenschein B, Schimansky-Geier L. Onset of synchronization in complex networks of noisy oscillators. Phys Rev E 2012;85:051116.
[23] Morelli LG, Zanette DH. Synchronization of stochastically coupled cellular automata. Phys Rev E 1998;58:R8–11.
[24] Iarosz KC, Bonetti RC, Batista AM, Viana RL, Lopes SR, Penna TJP. Supression of cancerous cells in cellular automaton. Pub UEPG (Impresso) 2010;16:79–85.
[25] Izhikevich EM. Simple model of spiking neurons. IEEE Trans Neural Network 2003;14:1569–72.
[26] Batista CAS, Lopes RS, Viana RL, Batista AM. Delayed feedback control of bursting synchronization in a scale-free neuronal network. Neural Networks 2010;23:114–24.
[27] Hodgkin AL, Huxley AF. A quantitative description of membrane current and its application to conduction and excitation in nerve. J Physiol 1952;117:500–44.
[28] Viana RL, Batista AM, Batista CAS, Pontes JCA, Silva FAS, Lopes SR. Bursting synchronization in networks with long-range coupling mediated by a diffusing chemical substance. Commun Nonlinear Sci Numer Simul 2012;17:2924.